Human Eye Response to Thermal Disturbances

Maryam Shafahi

Kambiz Vafai[1]
e-mail: vafai@engr.ucr.edu

Department of Mechanical Engineering,
University of California Riverside,
Riverside, CA 92521

Human eye is one of the most sensitive parts of the body when exposed to a thermal heat flux. Since there is no barrier (such as skin) to protect the eye against the absorption of an external thermal wave, the external flux can readily interact with cornea. The modeling of heat transport through the human eye has been the subject of interest for years, but the application of a porous media model in this field is new. In this study, a comprehensive thermal analysis has been performed on the eye. The iris/sclera section of the eye is modeled as a porous medium. The primary sections of the eye, i.e., cornea, anterior chamber, posterior chamber, iris/sclera, lens, and vitreous are considered in our analysis utilizing a two-dimensional finite element simulation. Four different models are utilized to evaluate the eye thermal response to external and internal disturbances. Results are shown in terms of temperature profiles along the pupillary axis. Effects of extreme ambient conditions, blood temperature, blood convection coefficient, ambient temperature, sclera porosity, and perfusion rate on different regions of the eye are investigated. Furthermore, the role of primary thermal transport mechanisms on the eye subject to different conditions is analyzed. [DOI: 10.1115/1.4002360]

Keywords: eye thermal modeling, eye thermal disturbance, bioheat, biological tissue, porous media, aqueous humor

1 Introduction

Thermal disturbances are more pronounced in the eye due to an insufficient blood flow circulation and lack of skin as a protecting layer. Lack of blood flow in the interior part of the eye makes it more vulnerable compared with other organs even in the case of weak thermal interactions.

Although recent noninvasive methods for temperature measurement of the eye, such as infrared (IR), are more convenient in comparison to the contact thermometry; only corneal temperature can be obtained using these methods. In biological systems, which are not amenable to direct investigation, such as human eye, computational modeling is the preferred tool to represent the transport phenomena [1–4]. Thermal modeling of the eye is important as it can provide one with a tool to investigate the effect of external heat sources as well as in predicting the abnormalities within the eye. Hot or cold weather can create a thermal load on the eye. Moreover, in order to optimize laser therapy or surgery in ophthalmology, it is essential to have a better understanding of the thermal response in different sections of the eye for an imposed heat flux.

In previous thermal models of the eye, heat transfer in different parts was primarily modeled using conduction and in a few cases by natural convection [2–12]. Ooi and Ng [2] studied the effect of aqueous humor (AH) hydrodynamics on the heat transfer within the eye. They also investigated the effect of different variables on the thermal modeling of the eye [3]. Chua et al. [5] modeled the impact of the aging of the human eye, thermal conductivity of the lens and a radiant flux on the temperature profile.

Lagendijk [6] performed experiments on the normal and heated rabbit eye and developed a conduction model to achieve the temperature distribution in human and rabbit eyes. Scott [8] utilized a 2D finite element method to obtain the temperature profile based on heat conduction in different sections of the eye. Effect of lens thermal conductivity, evaporation from cornea surface, blood flow in choroid, ambient temperature, ambient convection coefficient and blood temperature on the eye temperature distribution was studied based on a conduction model. Using a 2D model, Scott [9] also calculated the temperature change in intra-ocular media subject to an infrared radiation. Kumar et al. [10] developed a model to study the buoyancy effect on the convective motion for different geometrical configurations of a rabbit eye. Flyckt et al. [11] performed a comprehensive study on the cooling process of the eye by blood flow circulation. Amara [12] presented a conduction model to study the interaction between a laser flux and ocular media numerically. Jacobs [13] reviewed the multiscale hierarchical system of the eye considering the appropriate approaches to be taken to understand the complex properties and functions of the ocular tissues. Mapstone [14,15] recorded the cornea temperature subject to different ambient temperatures.

Although porous media models have been used in biomedical research [16–25], the previous investigations on the human eye did not utilize porous media modeling in representing the thermal transport. The first such attempt was done by the current authors at an ASME Heat Transfer Conference [1]. Porous media models have been utilized to study the characteristics of the bifurcation airflow and mass transfer within a lung [17], countercurrent bioheat transfer between terminal arteries and veins in the circulatory system [18], bioheat transport in biological media considering local thermal nonequilibruim [19,20], and arterial transport incorporating multi porous media layers [21,22].

The present work utilizes four pertinent thermal models to analyze heat transfer in six primary sections of the human eye. In model I, thermal transport occurs by conduction in all the domains. Model II accounts for natural convection in the anterior chamber; in model III iris/sclera is considered as a porous medium and model IV accounts for the existence of a porous medium and natural convection in anterior chamber. To the best of authors' knowledge, this is the first use of porous media modeling in analyzing the eye thermal characteristics and also the first comprehensive comparison among the pertinent thermal transport mechanisms within different regions of the eye.

2 Modeling and Formulation

2.1 Anatomy of the Eye. The eye is assumed to be a sphere with a given diameter. Its geometrical configuration such as thickness of the cornea, anterior chamber, lens, vitreous and sclera are

[1]Corresponding author.

Manuscript received March 25, 2010; final manuscript received April 1, 2010; published online September 30, 2010. Assoc. Editor: Andrey Kuznetsov.

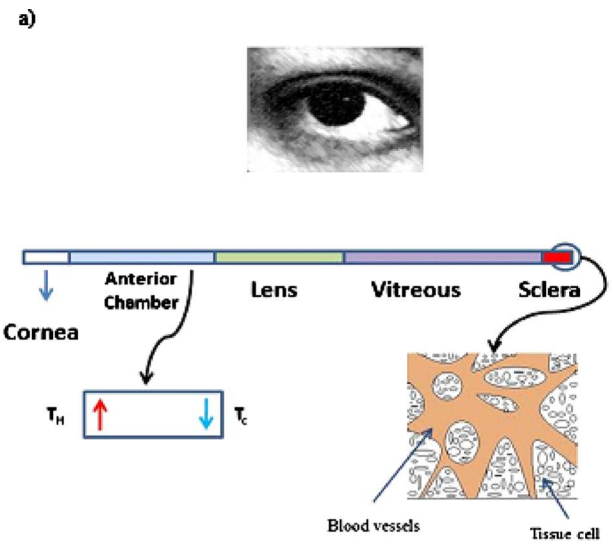

Fig. 1 Schematic of different primary sections of the eye along the pupillary axis: (*a*) different regions of the eye along the pupillary axis with a display of special attributes, (*b*) display of the primary regions within the eyeball, and (*c*) display of the blood/tissue interaction within Iris/sclera domain

based on the physiological data. There is blood flow in the iris/sclera part, which plays a crucial rule to adjust the eye temperature with the rest of the body. Different regions of the eye along the papillary axis with a display of special attributes as well as the two-dimensional eye configuration and display of the blood/tissue interaction within Iris/sclera domain are shown in Fig. 1.

2.2 Model I. In this model, conduction is assumed to be the dominant heat transfer mechanism in all of the subdomains of the eye. Each subdomain has its own thermal properties. The governing equation is as follows:

$$\rho_i c_i \frac{\partial T_i}{\partial t} = \nabla \cdot (k_i \nabla T_i) \quad i = a,b,c,d,e,f \tag{1}$$

where i denotes each subdomain in the eyeball. As shown in Fig. 1, a, b, c, d, e, and f refer to cornea, anterior chamber, lens, posterior chamber, vitreous and iris/sclera, respectively.

2.3 Model II. Model II accounts for the existence of AH in the anterior chamber. The energy transfer through this part occurs by both conduction and natural convection. The governing equations for five domains: cornea, posterior chamber, lens and vitreous regions are the same as that given in Eq. (1). The anterior chamber heat transfer is modeled as follows:

Continuity

$$\nabla \cdot \mathrm{v}_i = 0; \quad i = b \tag{2}$$

Momentum

$$\rho_i \frac{\partial \mathrm{v}_i}{\partial t} + \rho_i \mathrm{v}_i \nabla \cdot \mathrm{v}_i = -\nabla p_i + \rho_i g \beta_i (T_i - T_{\mathrm{ref}}); \quad i = b \tag{3}$$

The effect of buoyancy term is taken into account using the Boussinesq approximation, where β is the volume expansion coefficient and T_{ref} is the reference temperature.

The energy equation is as follows:

$$\rho_i c_i \frac{\partial T_i}{\partial t} - \nabla \cdot (k_i \nabla T_i) = -\rho c_i \mathrm{v}_i \,.\, \nabla T_i; \quad i = b \tag{4}$$

where the viscous dissipation effect is neglected.

2.4 Model III. Blood flow in the sclera/iris keeps the eye temperature close to the other body organs. This part is modeled as a porous medium while incorporating blood circulation through the tissue. Assuming a local thermal equilibrium between the blood and the tissue and accounting for the blood perfusion term, a modified Pennes equation is used in this work [16,21].

$$(1-\varphi_i)\rho_i c_i \frac{\partial T_i}{\partial t} = \nabla \cdot ((1-\varphi) k_i \nabla T_i) + \rho_b c_b \omega (T_{bl} - T_i); \quad i = f \tag{5}$$

Table 1 Summary of the pertinent equations utilized in the four primary eye thermal models

	Governing equations
Model I (conduction)	$\rho_i c_i \frac{\partial T_i}{\partial t} = \nabla \cdot (k_i \nabla T_i); \quad i = a,b,c,d,e,f$
Model II (conduction+natural convection)	$\rho_i c_i \frac{\partial T_i}{\partial t} = \nabla \cdot (k_i \nabla T_i); \quad i = a,c,d,e,f$
	$\nabla \cdot \mathrm{v}_i = 0; \quad i = b$
	$\rho_i \frac{\partial \mathrm{v}_i}{\partial t} + \rho_i \mathrm{v}_i \nabla \cdot \mathrm{v}_i = -\nabla p_i + \rho_i g \beta_i (T_i - T_{ref}); \quad i = b$
	$\rho_i c_i \frac{\partial T_i}{\partial t} - \nabla \cdot (k_i \nabla T_i) = -\rho c_i \mathrm{v}_i . \nabla T_i; \quad i = b$
Model III (conduction+porous media model)	$\rho_i c_i \frac{\partial T_i}{\partial t} = \nabla \cdot (k_i \nabla T_i); \quad i = a,b,c,d,e$
	$(1-\varphi_i)\rho_i c_i \frac{\partial T_i}{\partial t} = \nabla \cdot ((1-\varphi) k_i \nabla T_i) + \rho_{bl} c_{bl} \omega (T_{bl} - T_i); \quad i = f$
Model IV (conduction+natural convection+porous media model)	$\rho_i c_i \frac{\partial T_i}{\partial t} = \nabla \cdot (k_i \nabla T_i); \quad i = a,c,d,e$
	$\nabla \cdot \mathrm{v}_i = 0; \quad i = b$
	$\rho_i \frac{\partial \mathrm{v}_i}{\partial t} + \rho_i \mathrm{v}_i \nabla \cdot \mathrm{v}_i = -\nabla p_i + \rho_i g \beta_i (T_i - T_{ref}); \quad i = b$
	$\rho_i c_i \frac{\partial T_i}{\partial t} - \nabla \cdot (k_i \nabla T_i) = -\rho c_i \mathrm{v}_i . \nabla T_i; \quad i = b$
	$(1-\varphi_i)\rho_i c_i \frac{\partial T_i}{\partial t} = \nabla \cdot ((1-\varphi) k_i \nabla T_i) + \rho_{bl} c_{bl} \omega (T_{bl} - T_i); \quad i = f$

2.5 Model IV. In this model, the natural convection in anterior chamber and blood circulation in the iris/sclera as a porous medium are both accounted for. The governing equations are the same as model III in all the eye subdomains except anterior chamber, which follow the natural convection equations (Eqs. (2)–(4)).

2.6 Boundary Conditions. Radiation, evaporation and convection are accounted for at the cornea surface and the boundary condition for all the models on the cornea surface can be presented as follows:

$$n . (-k_i \nabla T_i) = E + h_{\mathrm{am}}(T_i - T_{\mathrm{am}}) + \sigma\varepsilon(T_i^4 - T_{\mathrm{am}}^4) \quad \text{on} \quad \Omega_i \quad i = a \tag{6}$$

where Ω_i is the external surface area corresponding to section i, E is the tear evaporation heat loss, and T_{am} and h_{am} are ambient temperature and convection coefficient, respectively.

At the sclera surface the thermal exchange between the eye ball and blood flow occurs through convection. The boundary condition at this interface can be presented as

$$n \cdot (k_i \nabla T_i) = h_{bl}(T_{bl} - T_i) \quad \text{on} \quad \Omega_i \quad i = f \tag{7}$$

Subdomains properties used in our simulations are based on the physiological data for the eye. A summary of the models utilized in the current work are given in Table 1. Different domain sizes and physical properties are taken from [2].

2.7 Numerical Solution. The domain is discretized using triangular elements with the Lagrange quadratic shape functions. The set of partial differential equations along with their related boundary conditions are coupled and are solved numerically by the finite element method using the commercial code COMSOL multiphysics program. The system of algebraic equations is solved with the Unsymmetric Multifrontal Method (UMFPACK) solver. The mesh independency has been verified by progressively increasing the number of elements insuring that the results are invariant. For example, increasing the number of elements from 5012 to 20,048 produced less than 1% change in the results.

3 Results and Discussion

The thermal analysis of the eye was carried out by utilizing four primary models. The eye response to various internal and external disturbances, such as fluctuations in blood temperature, blood convection coefficient, ambient temperature, ambient convection coefficient, extreme ambient conditions, iris/sclera porosity, and perfusion rate was investigated.

3.1 Comparison With Experimental Data. Models I–IV results are compared with the experimental data from Mapstone [14,15] and Lagrndijk [6] in Figs. 2 and 3. Lagendijk had assumed that the rabbit body temperature was 38.8°C and obtained the temperature of cornea, behind the lens, retina and rectal (within the sclera region) for a normal and heated rabbit eye. As Fig. 2

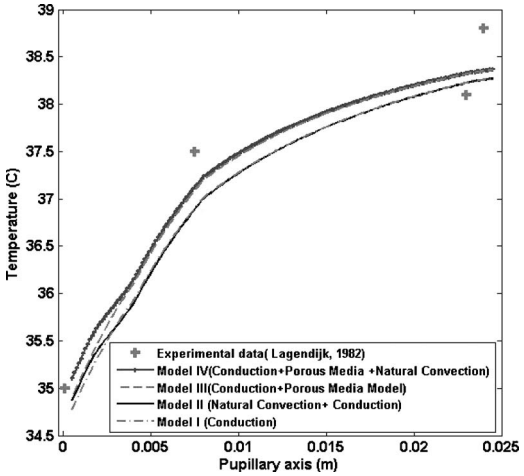

Fig. 2 Comparison of the analyzed models with Lagendijk's experimental data [6]; $h_{\mathrm{am}}=20$ W/m^2 K and $T_{\mathrm{am}}=25$°C

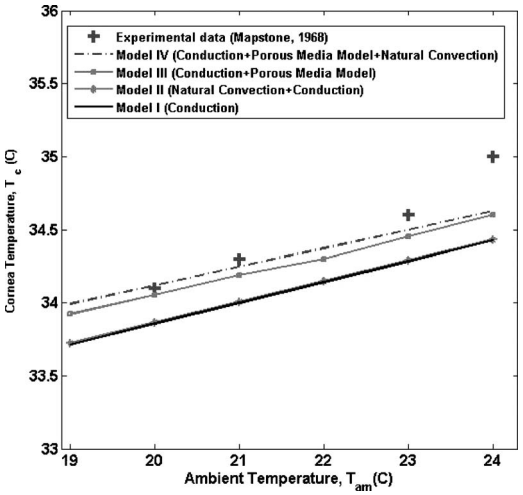

Fig. 3 Comparison of the analyzed models with Mapstone's experimental data [14]: h_{am}=10 W/m^2 K and E=40 W/m^2

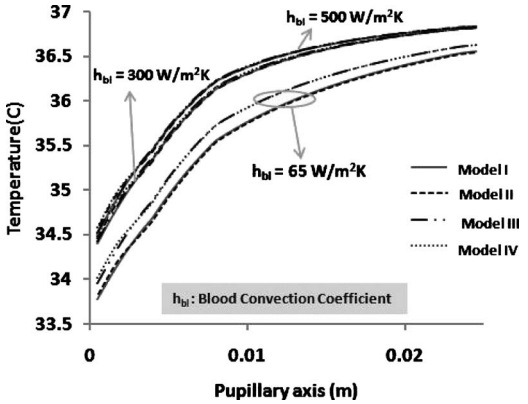

Fig. 5 Effect of blood convection coefficient on the pupillary axis temperature profile for the analyzed models; h_{am} =10 W/m^2 K and T_{am}=25°C

shows for a normal eye recorded temperatures are better estimated by porous media models. Overall, the two profiles provided by porous media models are in better agreement with the experimental data for the rabbit eye. Figure 3 shows the cornea temperature corresponding to different ambient temperatures. In this figure, model IV provides a very good match with the experimental observations. It should be noted that the temperature profiles from models I and II are approximately the same.

3.2 Effect of the Blood Temperature and Post Sclera Conditions. Blood circulation plays a crucial role in adjusting the eye temperature subject to a thermal load. In models I and II, blood circulation is taken into account only through the iris/sclera boundary conditions. In models III and IV, in addition to this boundary condition, the blood circulation is also directly taken into account through the perfusion term within the governing equations. This more closely mimics the physiological conditions. As can be seen in Fig. 4, models I and II predictions are almost identical when moving from anterior chamber toward sclera. Models III and IV show a smaller temperature gradient across the pupillary axis with an average temperature which is closer to the blood temperature. This is due to the presence of blood flow in the iris/sclera domain, which covers a substantial surface area of the eye ball as seen in Fig. 1(*c*). Figure 5 shows that for normal values of blood convection coefficient, there is a noticeable difference between the porous media models and models I and II. However, for very large blood convection coefficients, this difference diminishes significantly. This observation illustrates that the convective boundary condition on the iris/sclera surface has a substantial impact in all the models.

3.3 Effect Of Ambient Conditions. Figure 6 shows the effect of ambient convection coefficient on the pupillary axis temperature profile subject to a normal outside temperature. The eye thermal response to hot or cold ambient conditions is illustrated in Fig. 7. As can be seen, the porous media models provide a buffer against the outside thermal variations and result in an eye temperature distribution, which is closer to the temperature of the body. This is what is expected to occur based on biological information. It can be seen in these figures that the temperature profiles predicted by models, which account for the natural convection display a change in the curvature at the interface of the anterior chamber and the lens. For example, under cold ambient conditions given in Fig. 7(*b*), models II and IV result in cornea and anterior chamber temperatures, which are higher than those given by models I and III. This is due to the natural convection and formation of a circulatory cell within the anterior chamber. The dominant mechanism in the lens is conduction and for the cold ambient conditions, the higher temperature fluid in the anterior chamber transfers the thermal energy form the lens/AH interface toward the cornea/AH interface. This results in a temperature drop after the anterior chamber and the lens interface. Models I and III, which are only based on conduction in the cornea and the anterior cham-

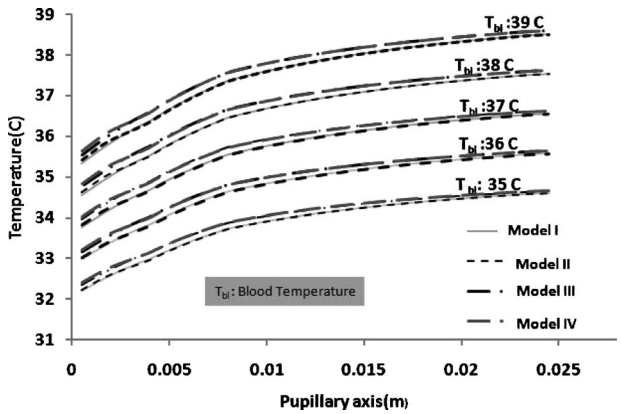

Fig. 4 Effect of the blood temperature on the pupillary axis temperature profile for the analyzed models; h_{am}=10 W/m^2 K and T_{am}=25°C

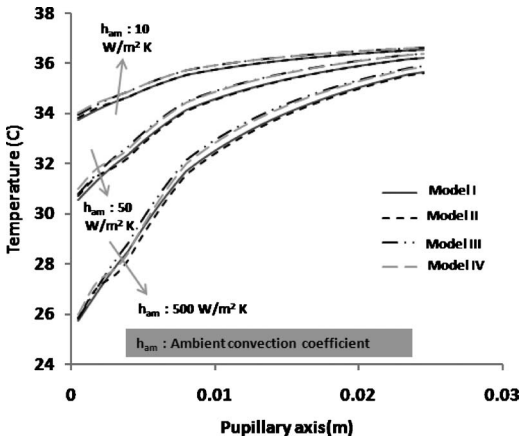

Fig. 6 Effect of the ambient convection coefficient h_{am} on the pupillary axis temperature profile for the analyzed models; T_{am}:25°C

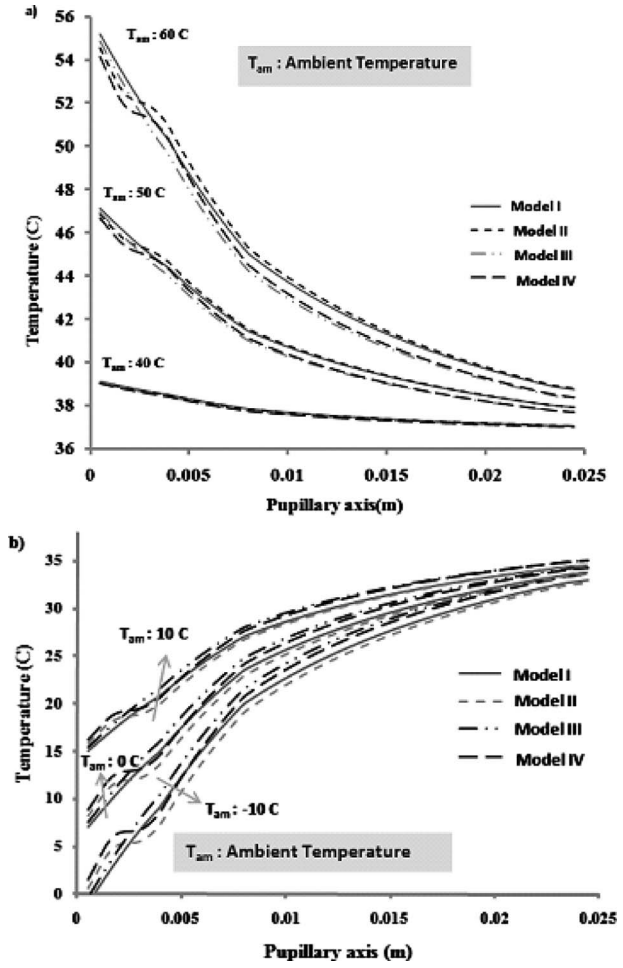

Fig. 7 Effect of the extreme ambient conditions on the eye thermal response along the pupillary axis: (*a*) hot ambient conditions T_{am}=40°C, 50°C, and 60°C; h_{am}=200 W/m^2 K and (*b*) cold ambient condition, T_{am}=−10°C, 0°C, 10°C; h_{am} =200 W/m^2 K

ber, produce a lower temperature in this region compared with those from models II and IV due to lack of this circulatory cell within the anterior chamber. The existence of the buoyancy cell for the cold ambient conditions can be seen in Fig. 8.

For the hot ambient conditions, the reverse of the described phenomena occurs as seen in Fig. 7(*a*). As it can be seen, the porous media models provide the proper buffer and result in the closest average temperature to the blood temperature for the eyeball for both extreme cold and hot ambient conditions within the cornea and the anterior chamber. This is expected to occur based on biological information. This observation shows that under extreme thermal disturbance, AH natural convection plays its own role to establish the eye ball temperature along with a substantial influence of blood circulation in the iris/sclera.

3.4 Effect of Aqueous Humor Flow Field on the Thermal Response of the Eye. Natural convection within the anterior chamber can play an important role in establishing the thermal response of the eye. In Fig. 9 the influence of ambient conditions on the velocity field within the anterior chamber for models II and IV are shown. It can be seen that when ambient convection coefficient changes from 50 W/m^2 K to 500 W/m^2 K, the maximum velocity within the anterior chamber increases by 50%. The presence of porous media in domain *f* affects the velocity field as it augments the movement within the natural convection cell, as can

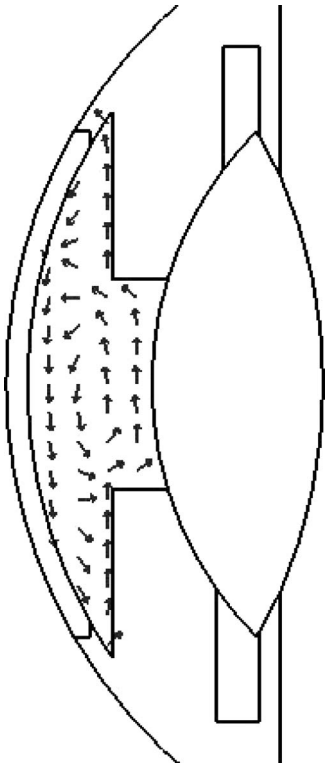

Fig. 8 Display of velocity distribution inside the anterior chamber when exposed to a cold ambient condition

be seen in Figs. 9(*d*)–9(*f*).

Natural convection in the anterior chamber maintains the temperature of the eye close to the other body organs when subjected to a thermal disturbance. When the thermal disturbance is more pronounced the differences among the four models becomes more noticeable.

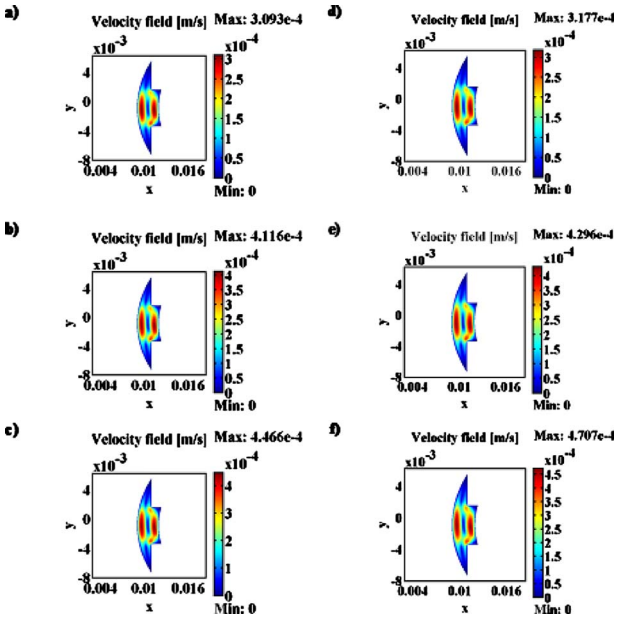

Fig. 9 Effect of the ambient convection coefficient on the velocity distribution within the anterior chamber for models II and IV; T_{am}=25°C. Model II: (*a*) h_{am}=50 w/m^2 K, (*b*) h_{am} =200 w/m^2 K, (*c*) h_{am}=500 w/m^2 K; model IV: (*d*) h_{am} =50 w/m^2 K, (*e*) h_{am}=200 w/m^2 K, and (*f*) h_{am}=500 w/m^2 K.

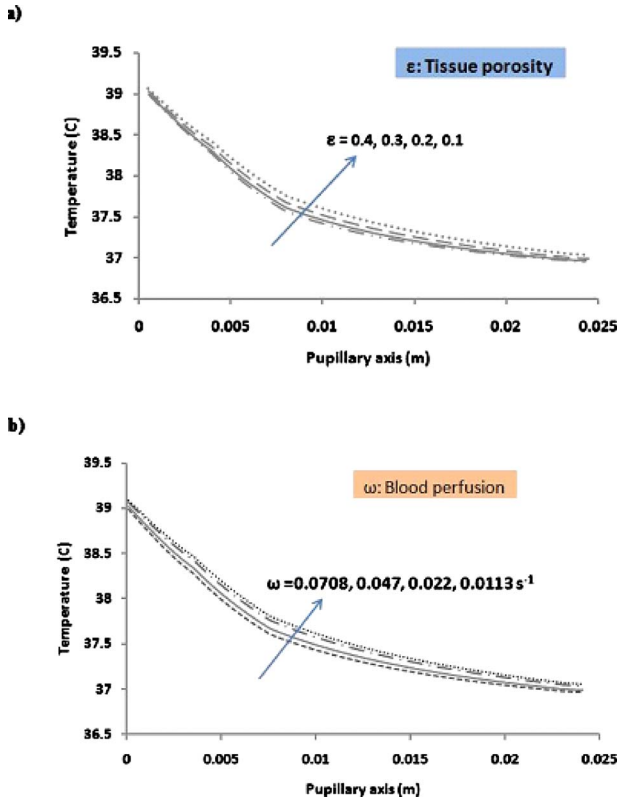

Fig. 10 Effect of variations in the iris/sclera characteristics on the eye thermal response along the pupillary axis for Model IV: (*a*) Effect of variations in tissue porosities and (*b*) effect of variations in blood perfusion rates; $h_{am}=200$ W/m^2 K and $T_{am}=40$°C

3.5 Effect of Iris/Sclera Porosity and Blood Perfusion Rate. As was mentioned earlier, Iris/sclera domain is considered as a porous medium with a given porosity and blood perfusion rate. As such the sclera/iris tissue characteristics has a significant influence on the thermal response of the eye. The effect of variations in the sclera domain porosity or perfusion rate on the temperature profile of the eye is shown in Figs. 10(*a*) and 10(*b*), respectively, for an ambient temperature of 40°C. It can be seen that an increase in either blood perfusion or porosity of the sclera enables the eye to better adapt to the internal body temperature.

4 Conclusions

The thermal response of a human eye to the internal and external disturbances was analyzed by investigating four primary thermal models. The effect of fluctuations in blood temperature, blood convection coefficient, ambient temperature, ambient convection coefficient, iris/sclera porosity, and blood perfusion rate on the temperature response for the eye was analyzed. The models, which were investigated in this study were compared with the available experimental data and the porous media models, were found to provide the best agreement. It was established that model IV, which includes the presence of blood circulation in the iris/sclera and hydrodynamics of AH region, maintains the closest temperature difference between the eyeball and the body organs when exposed to extreme thermal variations. The blood flow and AH circulation both have an important effect in adjusting the eyeball temperature. This effect becomes more pronounced for larger thermal disturbances, which is the case for cryosurgery and laser irradiation.

Nomenclature

- c = specific heat, J/kg K
- E = evaporation rate of tear, W/m^2
- H = convection coefficient, W/m^2 K
- k = thermal conductivity, W/m K
- n = normal vector
- p = pressure, Pa
- T = temperature, °C
- v = velocity, m/s

Greek Symbols

- ρ = density, kg/m^3
- μ = viscosity, Ns/m^2
- β = volume expansion coefficient, 1/K
- φ = porosity
- ω = perfusion rate, 1/s

Subscripts

- a = cornea
- am = ambient
- b = anterior chamber
- bl = blood
- c = lens
- d = posterior chamber
- e = vitreous
- f = iris/sclera
- i = subdomain index

References

[1] Shafahi, M., and Vafai, K., 2009, "Thermal Modeling of the Human Eye as a Porous Structure," ASME Paper No. HT2009-88138.
[2] Ooi, E., and Ng, E. Y. K., 2008, "Simulation of Aqueous Humor Hydrodynamics in Human Eye Heat Transfer," Comput. Biol. Med., **38**, pp. 252–262.
[3] Ng, E. Y. K., and Ooi, E. H., 2006, "FEM Simulation of the Eye Structure With Bioheat Analysis," Comput. Methods Programs Biomed., **82**, pp. 268–276.
[4] Narasimhan, A., Kumar Jha, K., and Gopal, L., 2010, "Transient Simulations of Heat Transfer in Human Eye Undergoing Laser Surgery," Int. J. Heat Mass Transfer, **53**, pp. 482–490.
[5] Chua, K. J., Ho, J. C., Chou, S. K., and Islam, M. R., 2005, "On the Study of the Temperature Distribution Within a Human Eye Subjected to a Laser Source," Int. Commun. Heat Mass Transfer, **32**, pp. 1057–1065.
[6] Lagendijk, J. J. W., 1982, "A Mathematical Model to Calculate Temperature Distribution in Human and Rabbit Eye During Hyperthermic Treatment," Phys. Med. Biol., **27**, pp. 1301–1311.
[7] Emery, A. F., Kramar, P., Guy, A. W., and Lin, J. C., 1975, "Microwave Induced Temperature Rises in Rabbit Eyes in Cataract Research," ASME J. Heat Transfer, **97**, pp. 123–128.
[8] Scott, J., 1988, "A Finite Element Model of Heat Transport in the Human Eye," Phys. Med. Biol., **33**, pp. 227–241.
[9] Scott, J., 1988, "The Computation of Temperature Rises in the Human Eye Induced by Infrared Radiation," Phys. Med. Biol., **33**, pp. 243–257.
[10] Kumar, S., Acharya, S., Beuerman, R., and Palkama, A., 2006, "Numerical Solution of Ocular Fluid Dynamics in a Rabbit Eye: Parametric Effects," Ann. Biomed. Eng., **34**, pp. 530–544.
[11] Flyckt, V. M. M., Raaymakers, B. W., and Lagendijk, J. J. W., 2006, "Modeling the Impact of Blood Flow on the Temperature Distribution in the Human Eye and the Orbit: Fixed Heat Transfer Coefficients Versus the Pennes Bioheat Model Versus Discrete Blood Vessels," Phys. Med. Biol., **51**, pp. 5007–5021.
[12] Amara, E. H., 1995, "Numerical Investigations on Thermal Effects of Laser–Ocular Media Interaction," Int. J. Heat Mass Transfer, **38**, pp. 2479–2488.
[13] Jacobs, M. D., 2009, "Multiscale Systems Integration in the Eye," WIREs Systems Biology and Medicine, **1**, pp. 15–27.
[14] Mapstone, R., 1968, "Determinants of Corneal Temperature," Br. J. Ophthalmol., **52**, pp. 729–741.
[15] Mapstone, R., 1968, "Measurement of Corneal Temperature," Exp. Eye Res., **7**, pp. 237–242.
[16] Nakayama, A., and Kuwahara, F., 2008, "A General Bioheat Transfer Model Based on the Theory of Porous Media," Int. J. Heat Mass Transfer, **51**, pp. 3190–3199.
[17] Kuwahara, F., Yoshihik, S., Jianjun, L., and Nakayama, A., 2009, "A Porous Media Approach for Bifurcating Flow and Mass Transfer in a Human Lung," ASME J. Heat Transfer, **131**, p. 101013.
[18] Nakayama, A., Kuwahara, F., and Liu, W., 2009, "A Macroscopic Model for Countercurrent Bioheat Transfer in a Circulatory System," J. Porous Media, **12**, pp. 289–300.
[19] Mahjoob, S., and Vafai, K., 2009, "Analytical Characterization of Heat Transfer Through Biological Media Incorporating Hyperthermia Treatment," Int. J. Heat Mass Transfer, **52**, pp. 1608–1618.

[20] Mahjoob, S., and Vafai, K., 2010, "Analysis of Bioheat Transport Through a Dual Layer Biological Media," ASME J. Heat Transfer, **132**, p. 031101.
[21] Khanafer, K., and Vafai, K., 2009, "Synthesis of Mathematical Models Representing Bioheat Transport," *Advances in Numerical Heat Transfer*, Vol. 3, W. J. Minkowycz and E. M. Sparrow, eds., Taylor & Francis, London, pp. 1–28.
[22] Khakpour, M., and Vafai, K., 2008, "A Critical Assessment of Arterial Transport Models," Int. J. Heat Mass Transfer, **51**, pp. 807–822.
[23] Khakpour, M., and Vafai, K., 2008, "A Comprehensive Analytical Solution of Macromolecular Transport Within an Artery," Int. J. Heat Mass Transfer, **51**, pp. 2905–2913.
[24] Khaled, A.-R. A., and Vafai, K., 2003, "The Role of Porous Media in Modeling Flow and Heat Transfer in Biological Tissues," Int. J. Heat Mass Transfer, **46**, pp. 4989–5003.
[25] Khanafer, K., and Vafai, K., 2006, "The Role of Porous Media in Biomedical Engineering as Related to Magnetic Resonance Imaging and Drug Delivery," Heat Mass Transfer, **42**, pp. 939–953.